ADVANCED ELECTRONIC MATERIALS
www.advelectronicmat.de

Polaronic Resistive Switching in Ceria-Based Memory Devices

*Lu Sun, Xiamin Hao, Qingling Meng, Ligen Wang, Feng Liu, and Miao Zhou**

Resistive random access memory (RRAM), or memristors, operating with a voltage-controlled low- and high-resistance state (ON/OFF), are a critical component for next-generation nanoelectronics. Most memristors are based on oxides, but the underlying working mechanism remains generally unclear. Using first-principles calculations, it is revealed that it is polaron that acts as the conducting species to mediate the resistive switching process in CeO_2, while the commonly believed oxygen vacancy (V_O^{2+}) plays only a secondary role in assisting polaron formation. Importantly, polaron and related complexes have desired low formation energies (≈–0.3 eV) and extremely small migration barriers (≈0.1 eV), to synergistically form conductive filaments in the CeO_2 matrix with shallow electronic states near Fermi level, while V_O^{2+} has a much higher migration energy and does not change the insulating nature of CeO_2. A switching field is also estimated of ≈3 V between the ON/OFF states from the relative stability of V_O^{2+}, H_{int}^+/H_{sub}^+ (institutional/substitutional hydrogen) and polaron complexes in reference to Fermi level, which agrees with experiments. The proposed polaron-based switching mechanism is general, paving the way for future understanding and design of multifunctional electronic nanodevices beyond RRAM.

Resistive random access memory (RRAM) devices, also referred to as memristors, are passive two-terminal circuit elements that can retain internal resistive state based on the history of applied voltage. The device concept was first proposed by Chua in 1971,[1] and has attracted widespread attention since 1990s. Memristors possess advantages of nonvolatility, high scalability, fast reading/writing operation, high-density integration, and excellent endurance.[2–4] They hold great promise for future construction of electronic architectures that can circumvent the von Neumann bottleneck.[5] Recently tremendous efforts have been made to designing and fabricating novel RRAM nanodevices with enhanced performance.[6–12]

Typical memristor adopts a metal-insulator-metal (MIM) configuration, in which an insulator film is sandwiched between two metal electrode layers. The electrode materials can be active metals such as Ag, Cu, and Ni, or inert metals such as Pt, Au, Pd, W, and TaN.[6–8,10,12] For the insulator film, a wide variety of materials have been proposed, including but not limited to electrolytes, doped organic semiconductors, amorphous Si and C, oxides and nitrides.[12] In this context, transition metal oxides, including TiO_2,[13] ZnO,[14] Ta_2O_5,[15] NiO,[16] CoO,[17] perovskite oxides such as $SrTiO_3$,[4] $Pr_{0.7}Ca_{0.3}MnO_3$,[18] and $Ba_{0.7}Sr_{0.3}TiO_3$,[19] and rare-earth oxides RE_2O_3 (RE = Y, Gd, Nd, Dy, Er)[20] have been most extensively explored for possible large-scale integrated circuits.

Cerium oxide (CeO_2) is a technologically important material with a broad range of applications in automotive exhaust, solid-oxide fuel cells and heterogeneous catalysts.[21–23] The presence of rich oxygen vacancies in CeO_2 endows it with exceptional oxygen storage and release capabilities. For these reasons, recent years have witnessed a surge of research pertaining to using CeO_2 as an insulating layer for memristive systems.[24–31] For instances, Hsieh et al.[24] reported RRAM in Al/CeO_x/Au with a low operating voltage and high resistance ratio, Kim[25] fabricated Pt/CeO_2/Pt device with resistance change >10^5 fold that mimics biological synaptic behaviors. Optimization of memristive performance has also been demonstrated by careful manipulation of oxygen vacancies via postannealing or doping of CeO_2.[26–28]

However, previous studies are all phenomenological in nature, and the physical mechanisms underlying RRAM are not clearly understood. Especially the creation/annihilation of conducting species responsible for the switching process remains unclear. A key challenge lies in the buried nature of conductive filament inside the oxide layer, which often involve sophisticated physical and chemical effects during switching between low-resistance (ON) and high-resistance (OFF) state. For MIM systems with active metal electrodes involving electrochemical

Dr. L. Sun, Prof. L. G. Wang
Materials Computation Center
General Research Institute for Nonferrous Metals
Beijing 100088, China
X. Hao, Q. Meng, Prof. M. Zhou
School of Physics
Beihang University
Beijing 100191, China
E-mail: mzhou@buaa.edu.cn
Prof. F. Liu
Department of Materials Science and Engineering
University of Utah
Salt Lake City, UT 84112, USA
Prof. F. Liu
Collaborative Innovation Center of Quantum Matter
Beijing 100084, China

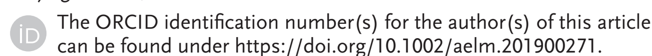
The ORCID identification number(s) for the author(s) of this article can be found under https://doi.org/10.1002/aelm.201900271.

DOI: 10.1002/aelm.201900271

 © 2019 WILEY-VCH Verlag GmbH & Co. KGaA, Weinheim

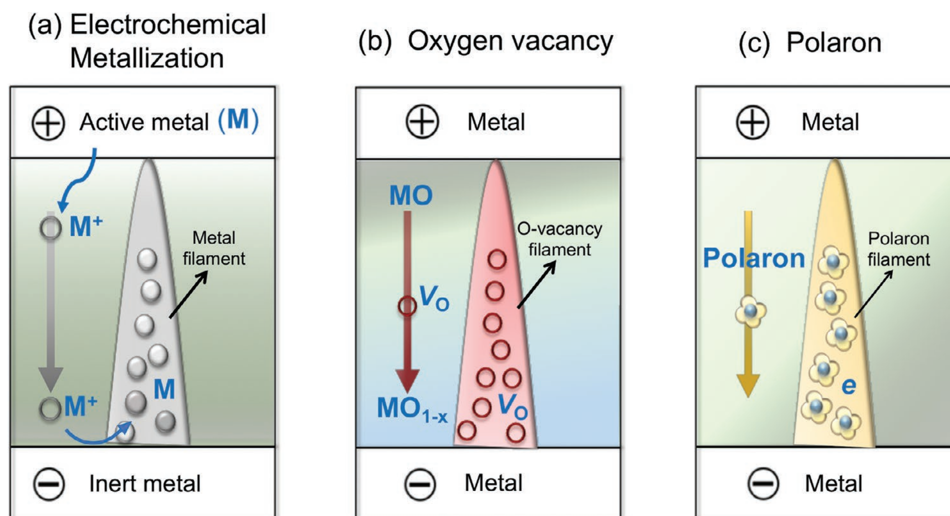

Figure 1. Schematics of two conventionally prevailing resistive switching mechanisms in RRAM devices involving a) electrochemical metallization and b) oxygen vacancy, in contrast with the new mechanism involving polaron c).

metallization (see **Figure 1**a), the active metal (M) is oxidized to metallic cations (M^+) that migrate toward the inert cathode and become reduced to metal at the electrode surface. Consequently, a conductive filament composed of metal species forms to switch the system to ON state. On the other hand, for many memristors that are based on oxides, oxygen vacancies (V_O^{2+}) are generally considered to be the dominant mobile species. It was suggested that migration of V_O^{2+} toward the cathode turns one region of the oxide layer into a nonstoichiometric state (MO_{1-x}, x = 0–1) forming a conductive filament to trigger the ON state (Figure 1b). However, as different defects usually exist in oxides, the exact mobile conducting species are difficult to be identified. Especially, formation and migration energies of V_O^{2+} are expected to be high and a microscopic picture of transport process remains lacking.

Here, using CeO_2 as a prototypical system, we reveal the physical mechanisms underlying a polaron-mediated resistive switching process in RRAM devices, as shown in Figure 1c. It was proposed in some previous experiments[28] that resistive switching effect in CeO_2 is based on migration of oxygen vacancies and polaron might also be involved. Surprisingly, we discover that in contrast with the common belief that oxygen vacancy forms the conductive filament, the CeO_2 with doubly ionized oxygen vacancy (V_O^{2+}) actually remains an insulating state so that V_O^{2+} cannot act as conducting species. Instead, polaron acts as the conducting species by inducing additional electronic states inside the energy gap of CeO_2, and hence disentangling the electronic conductivity from ionic contribution.[32–34] Most importantly, a low formation energy (≈–0.3 eV) and an extremely small migration barrier (<0.12 eV) renders synergistically a facile generation and migration of polarons to form the conductive filament in CeO_2 (Figure 1c). Furthermore, by comparing the formation energies of polaron and polaron complexes dressed with V_O^{2+}, interstitial and substitutional hydrogen (V_O^{2+}-polaron and H_{int}^+/H_{sub}^+-polaron) in reference to Fermi level, we are able to estimate a switching voltage of ≈3 V. These findings not only explain all the available experimental results,[24–31] but also shed new light on future design and fabrication of RRAM devices based on metal oxides with multivalence metal cations.

Bulk CeO_2 crystalizes in a cubic (fluorite) structure, which is an insulator with a wide bandgap of 3.3 eV.[35] As previous studies[36,37] suggested, screened hybrid functional is essential for correctly describing the energetic and electronic structures of CeO_2 and related systems. By using this sophisticated approach (computational details are shown in the Experimental Section), we calculated the orbital-projected density of states (DOS) of bulk CeO_2 (**Figure 2**a). The bandgap, between the occupied O 2p and unoccupied Ce 4f states, is 3.5 eV, in good agreement with the experimental value. We then evaluate the changing electronic structures of CeO_2 by introducing different defects. V_O^{2+} was generally accepted as the dominant conducting species for RRAM.[6–9,12] However, based on the DOS presented in Figure 2b, CeO_2 remains an insulating state in the presence of V_O^{2+}, as the O 2p-Ce 4f gap decreases by only 0.3 eV. Because single Ce vacancy is difficult to form due to a large formation energy (>7.0 eV), a key issue then arises pertaining to the exact defect species responsible for the conductivity. Small polaron in the form of Ce^{3+} species represents an intrinsic defect in CeO_2. It is characterized by electron localization in the 4f bands of Ce atoms accompanied by local structural distortion. As shown in Figure 2c, the polaron gives rise to a new occupied state located near the bottom of empty Ce 4f conduction band where the Fermi level resides. This signature strongly suggests that polaron can turn CeO_2 into a conductive state. Therefore, we propose that it is the small polaron, rather than oxygen vacancy, that acts as the conducting species to facilitate the switching process in RRAM devices.

Experiments have demonstrated the possibility of engineering resistive switching via controlled configurations and concentrations of oxygen vacancies.[26,27] We suggest that although V_O^{2+} does not change the conductivity of CeO_2, it can benefit the formation of polaron by donating electrons. Assuming each V_O^{2+} can bind with up to two polarons, forming singly positive (V_O^{2+}-1polaron)$^+$ or neutral (V_O^{2+}-2polarons)^0 complexes, we calculated the electronic structures of the two

© 2019 WILEY-VCH Verlag GmbH & Co. KGaA, Weinheim

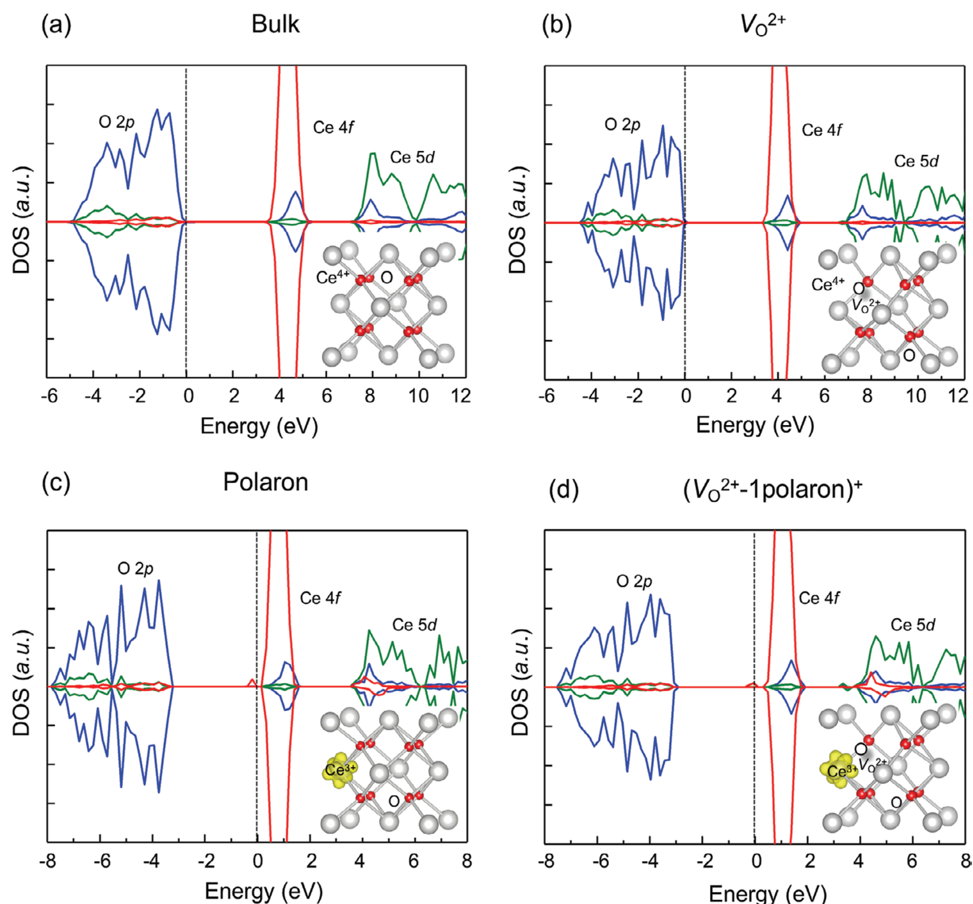

Figure 2. Partial DOS projected onto O 2p, Ce 5d, and 4f orbitals of CeO_2 in the presence of a) no defect, b) doubly ionized oxygen vacancy V_O^{2+}, c) small polaron Ce^{3+}, and d) singly positive $(V_O^{2+}\text{-1polaron})^+$ complex. Fermi level is set to zero (vertical dashed line). Inset in each figure shows the atomic configuration superimposed with charge density isosurfaces for polaron in (c) and (d) (isovalue = 0.05 e Å^{-3}). Large gray and small red spheres represent Ce and O atoms, respectively; dark hollow circles represent V_O^{2+}.

complexes. DOS of $(V_O^{2+}\text{-1polaron})^+$ and $(V_O^{2+}\text{-2polarons})^0$ are shown in Figure 2d and Figure S1 in the Supporting Information, respectively, from which one can clearly see additional occupied states appeared near Fermi level, rendering CeO_2 with good conductivity.

In practice, polarons can form with excess electrons contributed from both intrinsic defects, such as oxygen vacancies shown above, and also extrinsic charge donors present in the sample. Hydrogen is a common impurity in CeO_2,[38] which can be located at the interstitial site between O and Ce atoms, or a substituent replacing O. In both situations, H donates one electron to the system that tends to be localized close to nearby Ce atoms, favoring the formation of polaron. Indeed, our calculations show that interstitial H binds to the neighboring O atom with a bond length of ≈1.0 Å, and polaron sits close to the interstitial H, resulting in a neutral $(H_{int}^+\text{-1polaron})^0$ complex (**Figure 3**a). The substitutional H turns the neighboring Ce atom into Ce^{3+} state, leading also to the formation of a neutral $(H_{sub}^+\text{-1polaron})^0$ complex (Figure 3b). We calculated the DOS for the two cases, both of which exhibit pronounced electronic states near Fermi level, indicating again good electronic conductivity. However, with pure H_{int}^+ or H_{sub}^+ (when one electron is taken away so that no polaron forms), the system is insulating (see Figure S2 in the Supporting Information) just like CeO_2 with V_O^{2+}. All the above calculation results suggest that polaron and/or polaron complexes are responsible for the desired conductive electronic structures. Experimentally, it has been shown that resistive switching could be effectively tuned by H doping in TiO_2,[39] which we think is also related to the polaronic effect we propose here due to the presence of H.

We have further considered intrinsic defect complexes of larger size by creating more V_O^{2+}, so that more polarons can be introduced. In Figures S3 and S4 (Supporting Information), we show the detailed atomic configurations and partial DOS for $(2V_O^{2+}\text{-4polarons})^0$, $(3V_O^{2+}\text{-6polarons})^0$, $(4V_O^{2+}\text{-10polarons})^0$, and $(5V_O^{2+}\text{-10polarons})^0$ complexes. Our calculations indicate that these complexes tend to form complex clusters in CeO_2. Interestingly, larger complexes tend to produce more pronounced electronic states with a broadened width near Fermi level, and hence making CeO_2 more "metallic."

Next, we address the energetic properties of polaron and the associated defect complexes. The stability can be evaluated by the polaron formation energy, E^{form}, defined as the total energy difference between CeO_2 in a polaronic state and a reference state with an extra electron delocalized in the narrow 4f band, i.e., $E^{form} = E_{tot}(\text{polaron}) - E_{tot}(\text{delocalized})$. With this

© 2019 WILEY-VCH Verlag GmbH & Co. KGaA, Weinheim

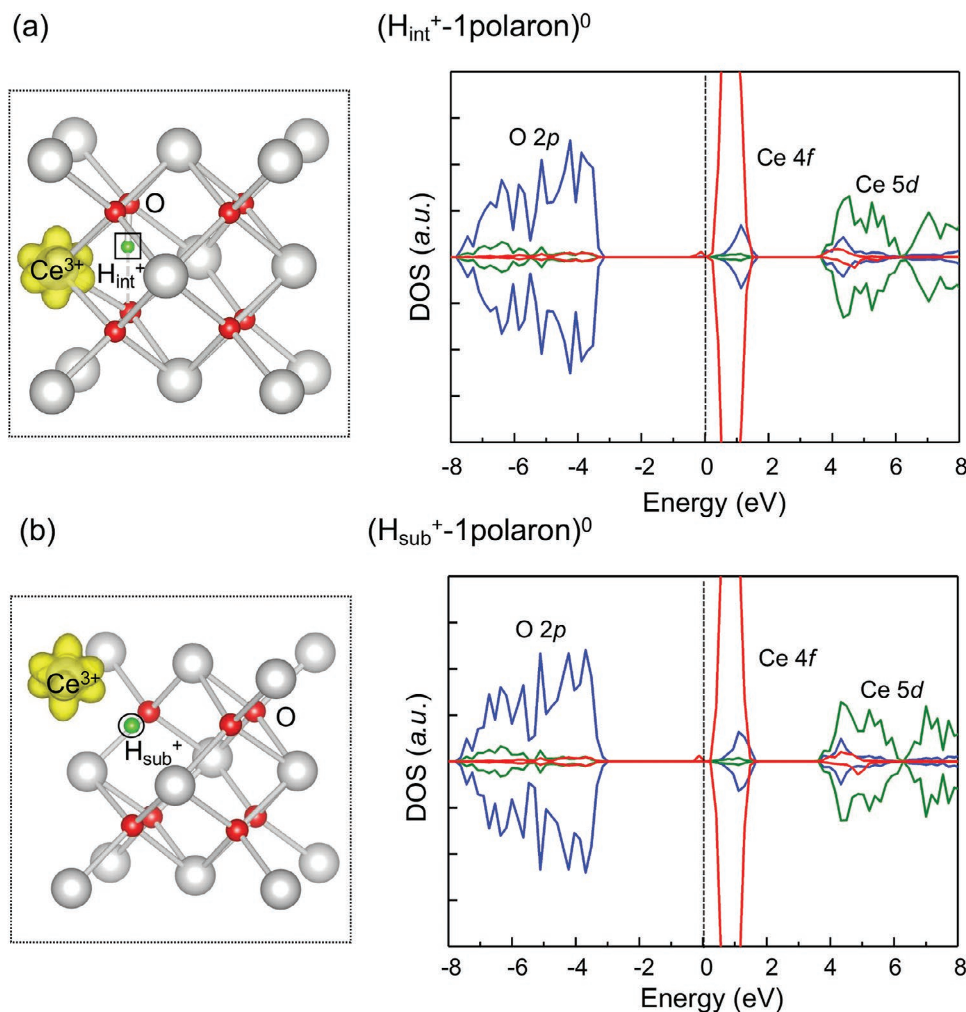

Figure 3. Calculated atomic configurations and partial DOS for a) neutral (H_{int}^{+}-1polaron)^0 and b) neutral (H_{sub}^{+}-1polaron)^0 complexes. H is represented by small green spheres. Isosurfaces of charge density for polarons are shown in yellow with an isovalue of 0.05 e Å^{-3}.

definition, negative E^{form} means that polaron is thermodynamically stable (exothermal). As listed in **Table 1**, the formation energy of a single polaron was calculated to be –0.304 eV, suggesting that electrons tend to be localized on Ce atom to form polaron. When a V_O^{2+} is present, the formation energy of polaron decreases to –0.362 eV, which further decreases significantly to –0.408 eV with two polarons. This suggests that V_O^{2+} enhances the formation of polarons in CeO_2, although V_O^{2+} by itself does not contribute to the conductivity. In the presence of H impurities, while H_{int}^{+} has negligible influence on the polaron formation energy, H_{sub}^{+} decreases the formation energy, and both can serve as the source of excess electron for the formation of polaron.

Table 1. Formation energies (E^{form}) of polaron in CeO_2 in presence of different donor species.

	E^{form} [eV]
Polaron	–0.304
(V_O^{2+}-1polaron)$^+$	–0.362
(V_O^{2+}-2polarons)^0	–0.408
(H_{int}^{+}-1polaron)^0	–0.298
(H_{sub}^{+}-1polaron)^0	–0.320

We have also calculated the formation energies of polaron complexes involving V_O^{2+}, H_{int}^{+}, and H_{sub}^{+} as a function of Fermi energy, in order to assess the effects of possible doping and external electric field on their relative stability. Here, in a charging state of q, the formation energy can be written as[37]

$$E^{form}(X^q) = E_{tot}(X^q) - E_{tot}(CeO_2) + \mu(X) + \mu_0(X) + q(E_{VBM} + E_F) + \Delta^q \quad (1)$$

where $E_{tot}(X^q)$ is the total energy of the supercell containing a defect X in a charging state q, and $E_{tot}(CeO_2)$ is the total energy of intrinsic CeO_2. The chemical potential μ(X) is the energy per atom of the defect reservoir, and μ_0(X) is the reference chemical potential. The Fermi level, which represents the energy of electronic reservoir, is a variable in this formalism in reference to the valence band maximum (E_{VBM}) of bulk CeO_2. Finally, Δ^q is the charging-state dependent correction due to the finite size of supercell. **Figure 4** presents the calculated formation energies for V_O^{2+}, H_{int}^{+}, H_{sub}^{+}, (V_O^{2+}-1polaron)$^+$, (V_O^{2+}-2polarons)^0,

© 2019 WILEY-VCH Verlag GmbH & Co. KGaA, Weinheim

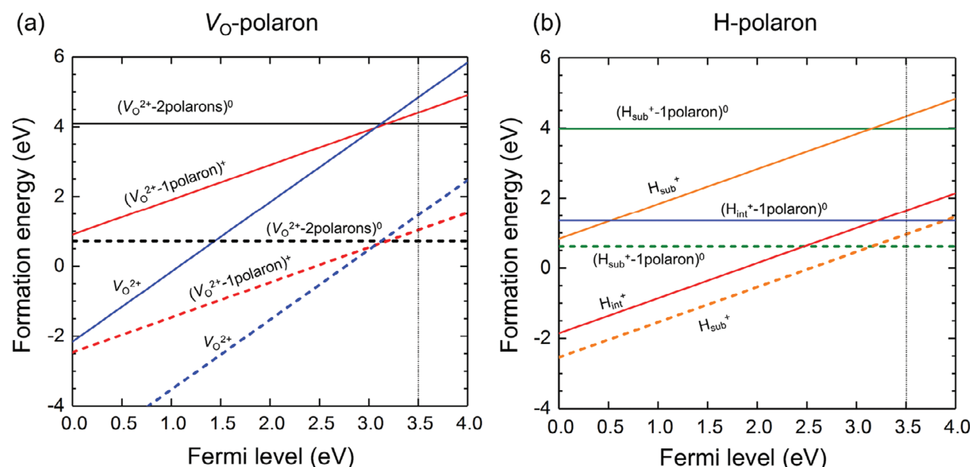

Figure 4. Calculated formation energies of a) V_O-polaron complexes and b) H-polaron complexes in different charging states as a function of Fermi level. Solid and dashed lines denote the oxygen-rich and oxygen-poor condition, respectively.

and $(H_{int/sub}^+$-1polaron$)^0$ complexes. Clearly, under oxygen-poor condition ($\mu_0 = -3.37$ eV), formation energies of V_O^{2+} and polaron complexes are all much smaller than those under oxygen-rich condition ($\mu_0 = 0$ eV). Over a large range of Fermi energy (0–3.0 eV), pure V_O^{2+} is the most stable defect, indicating the insulating nature of CeO_2, which corresponds to the OFF state in resistive switching process. As Fermi energy increases, more polarons are formed and $(V_O^{2+}$-2polaron$)^0$ complex becomes most stable when Fermi energy exceeds 3.1 eV (Figure 4a). As discussed above, CeO_2 with $(V_O^{2+}$-1polaron$)^+$ or $(V_O^{2+}$-2polarons$)^0$ are conductive, leading to an ON state. Similar behaviors were also found for CeO_2 with H impurities. As shown in Figure 4b, formation of H_{sub}^+ is energetically most stable (insulating, OFF) until Fermi energy exceeds 3.1 eV, where formation of $(H_{sub}^+$-1polaron$)^0$ prevails with a metallic feature, so that conductance emerges (ON). Therefore, the physical mechanism underlying the switching process in CeO_2 lies in the electric field controlled creation and annihilation of polarons in association with oxygen vacancies and/or H impurities, which decisively modulates the insulating/conducting nature of CeO_2. Remarkably, the calculated transition points of Fermi level for both V_O-polaron and H-polaron complexes, ≈3 eV, are in reasonable agreement with the experimentally reported switching voltages within a range of 2–4 V,[24,26,27,31] despite that switching voltage is dependent on the dielectric thickness, fabrication process as well as electrode materials.

We have thus far demonstrated the central role of polaron in modulating the electronic structures of CeO_2 and the stability of the polaron complex. Another key issue is its mobility in CeO_2, which dictates the kinetics of forming the conductive filament that determines the rate of switching process. To this end, we calculated the migration energy barriers of a single polaron and polaron in $(V_O^{2+}$-1polaron$)^+$, $(H_{int}^+$-1polaron$)^0$, and $(H_{sub}^+$-1polaron$)^0$ complexes. As a comparison, we also calculated the migration barrier of V_O^{2+} using the same model. **Figure 5** shows the migration barriers as well as the atomic configuration at the saddle point. Specifically, the migration process involves a polaron moving from one Ce_1^{3+} site to a neighboring Ce_2^{4+} site, turning them into Ce_1^{4+} and Ce_2^{3+}, respectively, i.e., Ce_1^{3+}-$Ce_2^{4+} \rightarrow Ce_1^{4+}$-$Ce_2^{3+}$. During this process, the excess electron is gradually transferred from Ce_1 to Ce_2 site, and the saddle point occurs at the middle point of initial and final configurations, where electrons are equally distributed between the two Ce atoms.

As shown in Figure 5, the migration barrier of a single polaron is 0.12 eV, which is very small, indicating a facile migration of polaron in CeO_2. In comparison, the migration barrier of single V_O^{2+} is 0.47 eV, about four times larger than that of polaron. One can estimate their respective mobility μ at temperature T by, $\mu \propto 1/T \exp(-E_a/k_BT)$,[40] where E_a is the activation energy (migration barrier) and k_B is the Boltzmann constant. The mobility of polaron is found six orders of magnitude larger than that of V_O^{2+} at room temperature (300 K). Remarkably, with the presence of V_O^{2+}, the migration barrier of polaron is further decreased to 0.07 by 0.05 eV relative to a single polaron (0.12 eV). Thus, oxygen vacancies greatly promote the migration of polarons. This implies an intriguing

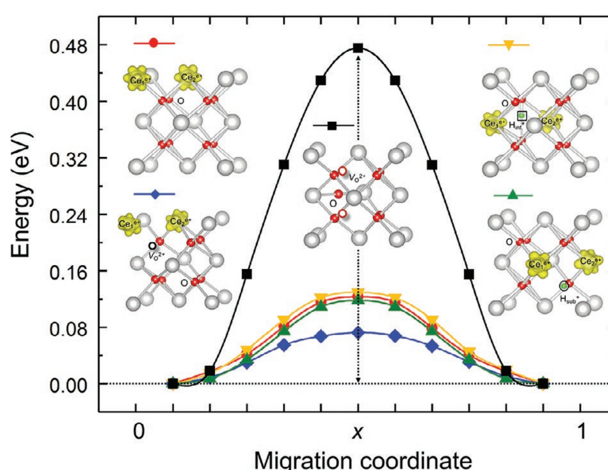

Figure 5. Migration profiles of single V_O^{2+}, polaron, polaron complexes with V_O^{2+}, H_{int}^+, and H_{sub}^+ in CeO_2, which are denoted by dark squares, red circles, blue diamonds, green regular triangles, and orange inverted triangles, respectively. Inset structures are the corresponding atomic configurations at the saddle point, superimposed with charge density isosurfaces for polaron (isovalue = 0.05 e Å^{-3}).

© 2019 WILEY-VCH Verlag GmbH & Co. KGaA, Weinheim

synergistic effect existing in such (V_O^{2+}-1polaron)$^+$ complex that are both thermodynamically and kinetically favored to achieve resistive switching. In contrast, hydrogen impurities, for both H_{int}^+ and H_{sub}^+, were found to have little influence on polaron migration barrier, consistent with their effects on formation energy (see Table 1).

In experiments, it is rather difficult to image the exact defect species that form the conductive filaments during switching process. However, there are experimental reports on oxide-based memristive devices that have indirectly suggested the importance of polaron in switching process. For instances, Foglietti et al. studied the conductive filaments in Nb:$SrTiO_3$/CeO_2/Pt device, and explained the possible electronic transport by occupation of thermally injected electrons on Ce 4f levels under applied electric fields.[41] Wang et al. measured thermoelectric Seebeck coefficient that reflects the electronic properties of conductive filaments in Ti/HfO_x/Pt device, who described the electronic transport by using polaron hopping model.[42] Yim et al. provided clear scanning tunneling microscopy images on the polaronic character of electron distribution around oxygen vacancies in TiO_2, and suggested that the electric field tuned polarons may allow the construction of conduction pathways.[43] Therefore, these experiments support the polaronic switching mechanism in oxide-based memristive devices as we propose here.

To summarize, we have demonstrated a new mechanism of resistive switching in ceria-based RRAM by revealing the central role of polaron in generating the conductive characteristics of CeO_2. Our calculations show that it is polaron complex, rather than oxygen vacancy as perceived before, that acts as the "conductive species" in CeO_2. They are characterized with additional electronic states inside the energy gap near Fermi level. Remarkably, the relative stability of V_O^{2+}, H_{int}^+, H_{sub}^+, and polaron complexes can be effectively controlled by external electrical field to readily achieve an ON/OFF switching, which not only quantitatively explains experimental observations, but also quantitatively agrees with an experimental switching voltage of ≈3 V. We believe the polaron-mediated resistive switching mechanism is general, applicable to a wide range of metal oxides with multivalence cations, such as TiO_2, HfO_2, and Ta_2O_5, which may shed new light on future fabrication and design of oxide-based memristive devices for various applications.

Experimental Section

The energetic and electronic structure calculations were performed in the framework of density functional theory, using the projector-augmented wave method with spin-polarization[44] as implemented in the Vienna Ab Initio Simulation Package (VASP).[45,46] The Ce ($5s^25p^65d^14f^16s^2$) and O ($2s^22p^4$) electrons were treated as valence states, and employed the screened hybrid functional of Heyd, Scuseria, and Ernzerhof (HSE06), which mixed 75% of the generalized gradient approximation in Perdew–Burke–Ernzerhof exchange and 25% of the nonlocal Hartree–Fock exchange.[47] The screening parameter that separates the exchange potential into short and long range parts was set 0.2.[47] To simulate V_O, H impurity and polaron in CeO_2, a $2 \times 2 \times 2$ supercell of CeO_2 was used. The equilibrium lattice parameters of CeO_2 was calculated to be 5.40 Å by HSE06, in good agreement with the experimental value of 5.41 Å.[48] Integrations over the Brillouin zone of the supercell were performed using the (1/4, 1/4, 1/4) special-k point. A larger supercell of $3 \times 3 \times 3$ was used to calculate the complexes of larger size. The energy cutoff for the plane-wave basis was set to 300 eV due to the high computational cost, and tests for the formation energy using a cutoff of 400 eV were also performed to ensure convergence. All structures were relaxed until the forces on each atom were lower than 0.01 eV Å^{-1}.

Supporting Information

Supporting Information is available from the Wiley Online Library or from the author.

Acknowledgements

This work was supported by the Science Challenge Project (TZ2018004), the National Natural Science Foundation of China (Grant Nos. 51601116, 11674042, and 11804293). F.L. acknowledges support by U.S. DOE-BES (Grant No. DE-FG02-04ER46148). The authors also acknowledge the support from the Thousand Youth Talents Program of China.

Conflict of Interest

The authors declare no conflict of interest.

Keywords

cerium oxide, conductive filaments, memristive switching, polaron, synergistic effects

Received: March 12, 2019
Revised: June 4, 2019
Published online:

[1] L. O. Chua, *IEEE Trans. Circuit Theory* **1971**, *18*, 507.
[2] A. Asamitsu, Y. Tomioka, H. Kuwahara, Y. Tokura, *Nature* **1997**, *388*, 50.
[3] A. Beck, J. G. Bednorz, C. Gerber, C. Rossel, D. Widmer, *Appl. Phys. Lett.* **2000**, *77*, 139.
[4] Y. Watanabe, J. G. Bednorz, A. Bietsch, Ch. Gerber, D. Widmer, A. Beck, S. J. Wind, *Appl. Phys. Lett.* **2001**, *78*, 3738.
[5] D. B. Strukov, G. S. Snider, D. R. Stewart, R. S. Williams, *Nature* **2008**, *453*, 80.
[6] R. Waser, M. Aono, *Nat. Mater.* **2007**, *6*, 833.
[7] A. Sawa, *Mater. Today* **2008**, *11*, 28.
[8] R.Waser, R. Dittmann , G. Staikov, K. Szot, *Adv. Mater.* **2009**, *21*, 2632.
[9] H. Akinaga, H. Shima, *Proc. IEEE* **2010**, *98*, 2237.
[10] I. Valov, R. Waser, J. R. Jameson, M. N. Kozicki, *Nanotechnology* **2011**, *22*, 254003.
[11] D. S. Jeong, R. Thomas, R. S. Katiyar, J. F. Scott, H. Kohlstedt, A. Petraru, C. S. Hwang, *Rep. Prog. Phys.* **2012**, *75*, 076502.
[12] J. J. Yang, D. B. Strukov, D. R. Stewart, *Nat. Nanotechnol.* **2013**, *8*, 13.
[13] J. J. Yang, M. D. Pickett, X. M. Li, D. A. A. Ohlberg, D. R. Stewart, R. S. Williams, *Nat. Nanotechnol.* **2008**, *3*, 429.
[14] W. Y. Chang, Y. C. Lai, T. B. Wu, S. F. Wang, F. Chen, M. J. Tsai, *Appl. Phys. Lett.* **2008**, *92*, 022110.
[15] T. Sakamoto, K. Lister, N. Banno, T. Hasegawa, K. Terabe, M. Aono, *Appl. Phys. Lett.* **2007**, *91*, 092110.

© 2019 WILEY-VCH Verlag GmbH & Co. KGaA, Weinheim

[16] S. H. Chang, J. S. Lee, S. C. Chae, S. B. Lee, C. Liu, B. Kahng, D. W. Kim, T. W. Noh, *Phys. Rev. Lett.* **2009**, *102*, 026801.
[17] K. Nagashima, T. Yanagida, K. Oka, M. Taniguchi, T. Kawai, J. S. Kim, B. H. Park, *Nano Lett.* **2010**, *10*, 1359.
[18] Y. B. Nian, J. Strozier, N. J. Wu, X. Chen, A. Ignatiev, *Phys. Rev. Lett.* **2007**, *98*, 146403.
[19] R. Oligschlaeger, R. Waser, R. Meyer, S. Karthauser, R. Dittmann, *Appl. Phys. Lett.* **2006**, *88*, 042901.
[20] T. M. Pan, C. H. Lu, *Appl. Phys. Lett.* **2011**, *99*, 5655.
[21] J. Kašpar, P. Fornasiero, M. Graziani, *Catal. Today* **1999**, *50*, 285.
[22] K. Eguchi, T. Setoguchi, T. Inoue, H. Arai, *Solid State Ionics* **1992**, *52*, 165.
[23] Q. Fu, H. Saltsburg, M. Flytzani-Stephanopoulos, *Science* **2003**, *301*, 935.
[24] C. C. Hsieh, A. Roy, A. Rai, Y. F. Chang, S. K. Banerjee, *Appl. Phys. Lett.* **2015**, *106*, 173108.
[25] H. J. Kim, H. Zheng, J. S. Park, D. H. Kim, C. J. Kang, J. T. Jang, D. H. Kim, T. S. Yoon, *Nanotechnology* **2017**, *28*, 285203.
[26] A. Younis, D. Chu, S. Li, *J. Phys. D: Appl. Phys.* **2012**, *45*, 355101.
[27] R. Schmitt, J. Spring, R. Korobko, J. L. M. Rupp, *ACS Nano* **2017**, *11*, 8881.
[28] P. Gao, Z. Wang, W. Fu, Z. Liao, K. Liu, W. Wang, X. Bai, E. Wang, *Micron* **2010**, *41*, 301.
[29] M. Yoshitake, M. Vaclavu, M. Chundak, V. Matolin, T. Chikyow, *J. Solid State Electrochem.* **2013**, *17*, 3137.
[30] M. Ismail, C. Y. Huang, D. Panda, C. J. Huang, T. L. Tsai, J. H. Jieng, C. A. Lin, U. Chand, A. M. Rana, E. Ahmed, I. Talib, M. Y. Nadeem, T. Y. Tseng, *Nanoscale Res. Lett.* **2014**, *9*, 45.
[31] D. C. Kakushima, K. Ahmet, K. Tsutsui, A. Nishiyama, N. Sugii, K. Natori, T. Hattori, H. Iwai, *Microelectron. Reliab.* **2012**, *52*, 688.
[32] M. Mogensen, T. Lindegaard, U. R. Hansen, G. Mogensen, *J. Electrochem. Soc.* **1994**, *141*, 2122.
[33] H. L. Tuller, A. S. Nowick, *J. Phys. Chem. Solids* **1977**, *38*, 859.
[34] D. S. Park, J. Griffith, A. S. Nowick, *Solid State Ionics* **1981**, *2*, 95.
[35] E. Wuilloud, B. Delley, W. D. Schneider, Y. Baer, *Phys. Rev. Lett.* **1984**, *53*, 202.
[36] L. Sun, W. Xiao, X. Hao, Q. Meng, M. Zhou, *Electron. Struct.* **2019**, *1*, 015003.
[37] L. Sun, X. Huang, L. Wang, A. Janotti, *Phys. Rev. B* **2017**, *95*, 245101.
[38] K. Sohlberg, S. T. Pantelides, S. J. Pennycook, *J. Am. Chem. Soc.* **2001**, *123*, 6609.
[39] J. R. Jameson, Y. Nishi, *Integr. Ferroelectr.* **2011**, *124*, 112.
[40] S. D. Kang, M. Dylla, G. J. Snyder, *Phys. Rev. B* **2018**, *97*, 235201.
[41] V. Foglietti, N. Yang, C. Aruta, F. D. Pietrantonio, D. Cannata, M. Benetti, G. Balestrino, *Nanotechnology* **2016**, *27*, 375705.
[42] M. Wang, C. Bi, L. Li, S. Long, Q. Liu, H. Lv, N. Lu, P. Sun, M. Liu, *Nat. Commun.* **2014**, *5*, 4598.
[43] C. M. Yim, M. B. Watkins, M. J. Woff, C. L. Pang, K. Hermansson, G. Thornton, *Phys. Rev. Lett.* **2016**, *117*, 116402.
[44] P. E. Blochl, *Phys. Rev. B* **1994**, *50*, 17953.
[45] G. Kresse, J. Hafner, *Phys. Rev. B* **1993**, *47*, 558.
[46] G. Kresse, J. Furthmüller, *Comput. Mater. Sci.* **1996**, *6*, 15.
[47] a) J. Heyd, G. E. Scuseria, M. J. Ernzerhof, *Chem. Phys.* **2003**, *118*, 8207; b) *J. Chem. Phys.* **2006**, *124*, 219906.
[48] J. Gerwand, J. S. Olsen, L. Petit, G. Vaitheeswaran, V. Kanchana, A. Svane, *J. Alloys Compd.* **2005**, *400*, 56.

© 2019 WILEY-VCH Verlag GmbH & Co. KGaA, Weinheim